Int. J. Electrochem. Sci., 16 **(2021)** Article ID: 210561, doi: 10.20964/2021.05.36

International Journal of
ELECTROCHEMICAL
SCIENCE
www.electrochemsci.org

Iron and Nitrogen Co-doped Carbon Spheres as High Efficiency Oxygen Reduction Catalyst

Zhaoyan Chen[1], Supeng Pei[1,], Yueyang Sun [1], Xia Xiong [1], Wei Zhang[1], Zhiyue Han[1], Kangwei Xu[1], Zongshang Zhou[1], Yongming Zhang[2,3], Wei Feng[3], Li Wang [3], YeCheng Zou[3]*

[1] School of Chemical and Environmental Engineering, Shanghai Institute of Technology, Shanghai 201418, China.
[2] School of Chemistry and Chemical Engineering, Center of Hydrogen Science, Shanghai Jiao Tong University, Shanghai 200240, China.
[3] State Key Laboratory of Fluorinated Functional Membrane Materials, Dongyue Group, Zibo 256401, China.
[*]E-mail: peisupeng@126.com

Received: 7 November 2020 / *Accepted:* 16 December 2020 / *Published:* 31 March 2021

Iron and nitrogen co-doped carbon spheres (Fe-N/CS) catalysts were prepared from iron nitrate nonahydrate by electrospinning and thermal treatment. The effect of different iron contents on the morphology and performance of the catalyst was explored by changing the amount of iron precursor. And the relationship between its structure and the oxygen reduction activity was also discussed. The results showed that there is an optimal content for the iron. When the iron content was 0.18% (Fe-N/CS-0.18), the initial and half-wave potential of the catalyst were 0.970 V and 0.842 V, which are the best result among the Fe- N/CS catalysts. Compared with that for commercial Pt/C, the Fe-N/CS-0.18 even showed a better ORR catalytic performance. The current retention of the Fe-N/CS-0.18 was 90.6% after continuous operation for 10000 s, which is better than that for commercial Pt/C（84.2%）. Additionally, the methanol tolerance of Fe-N/CS-0.18 is better than that of the commercial Pt/C. The current density percentage of Fe-N/CS-0.18 has slightly decrease after the addition of methanol at 500 s. However, the commercial Pt/C decreases sharply. This was attributed to the abundant active nitrogen (pyridine nitrogen and pyrrole nitrogen) and suitable iron content in Fe-N/CS-0.18, which easily promote the oxygen reduction reaction.

Keywords: Iron-nitrogen codoped; Carbon sphere; Oxygen reduction catalyst

1. INTRODUCTION

Polymer electrolyte membrane fuel cells (PEMFC) have been widely used in fuel cells account for their long service life, low electrolyte operating temperature, fast start-up speed, environmental

friendliness, and high working current density[1-4]. Although proton exchange membrane fuel cells have been used on a small scale, they have not yet been commercialized on a large scale. The primal problem is the precious cost and short service life of the cathode catalyst. Therefore, the development of new and efficient catalysts for proton exchange membrane fuel cells has become a topic of interest in the research of proton exchange membrane fuel cells[5, 6]. In PEMFCs, the cathodic oxygen reduction reaction (ORR) is a complex electrochemical reaction involving many steps, and its reaction kinetics are slow[7-9]. Currently, platinum-based catalysts and their alloy catalysts are the catalysts with the most active for ORR. Nevertheless, Platinum as the main cathode catalyst needs to solve the problem of its high cost[10-14].

Catalysts are one of the core components of proton exchange membrane fuel cells, especially cathodic ORR catalysts[15, 16]. Therefore, the development of new non-noble metal/nonmetal catalysts to increase the rate of the oxygen reduction reaction and reduce the cost of catalysts has become one of the main issues to solve to promote the rapid development of fuel cells[17-19].

At present, various metal-nitrogen co-doped carbon materials have been utilized in oxygen reduction catalysts, and the doped non-noble metals are usually iron, cobalt, nickel, copper or manganese[20-23]. These studies mainly focus on optimizing the preparation conditions and modulating the structure of the compounds to obtain the maximum catalyst activity and stability. It is found that the iron-nitrogen co-doped catalyst carbon materials (Fe-N/C) were tested in alkaline media with excellent oxygen reduction performances[24-26]. Nevertheless, the reason that the activity and stability of iron-nitrogen co-doped catalysts are enhanced after treatment is still unclear, and a substantial amount of effort has been made to understand these issues. Besides, the morphology and specific surface area of the catalyst are significant factors affecting the activity of the catalyst[27]. The content and species of nitrogen and active metals are also vital factors that impact catalytic activity[28, 29].

As a simple and versatile strategy, the electrospinning technique has gained popularity to fabricate nano- or micron-sized materials[30, 31]. This work is further improved on the basis of our previous work[32] and the iron and nitrogen co-doped carbon spheres (Fe-N/CS) catalysts were prepared by electrospinning and thermal treatment. To explore the impact of the iron content in the catalysts, the four catalysts with different iron content have been synthesized by changing the amount of added iron nitrate nonahydrate. Furthermore, the influence of the structure of the doped carbon spheres and the oxygen reduction performance of the catalysts was determined.

2. EXPERIMENTAL DETAIL

2.1 Materials

The main raw materials comprised iron nitrate nonahydrate, polyacrylonitrile (PAN), polyvinylpyrrolidone (PVP), gas-phase silica and dimethyl formamide (DMF). Analytical grade Iron nitrate nonahydrate was purchased from China Pharmaceutical Group Co., Ltd. The PAN (MW~150000 g mol^{-1}) was received from Solvay S.A. The PVP (Mw~5500 g mol^{-1}) was bought from Shanghai Qifu Materials Tech Co., Ltd. The DMF and gas-phase silica were purchased from Shanghai Lingfeng

Chemical Reagent Co., Ltd. All solvents and chemicals were utilized as received without any further purification.

2.2 Preparation of Fe-N codoped carbon sphere (Fe-N/CS) catalysts

The Fe-N/CS catalysts were prepared by a typical procedure, a certain amount of Iron nitrate nonahydrate, 0.5 g polyacrylonitrile (PAN), 0.5 g polyvinylpyrrolidone (PVP) and 0.428 g gas-phase silica were dissolved in 9 g N, N-dimethyl formamide (DMF) simultaneously. Part of the solution was transferred to a 2.5 mL disposable syringe, and the syringe was placed on the electrostatic spinning apparatus. Precursors with different iron contents(the addition of iron nitrate nonahydrate is 90.5 mg , 181mg, 271.5 mg and 362 mg, respectively） were prepared by the electrostatic spinning method to obtain polymer nanofilms. The liquid speed was set at 0.05 ml/h, the spinning voltage was set at 12 kV, and an aluminum foil was placed 15 cm below the spinner. Then, the prepared polymer fiber membrane was placed in a 60℃ oven to dry for 2 h to evaporate the volatile solvent, and then the fiber membrane was placed in a porcelain boat in a tube furnace for baking. The heat treatment was performed at a heating rate of 2℃/min in air for 2 h at 220℃. After waiting for the sample to cool to room temperature, the final product was carbonized at 800℃ at a rate of 2℃/min for 2 hours under the protection of nitrogen. The calcined product was placed in a 10% HF solution and stirred for 8 hours, and then filtered and washed until the solution was neutral. According to the amount of iron nitrate nonahydrate added, the samples were named N/CS, Fe-N/CS-0.07, Fe-N/CS-0.13, Fe-N/CS-0.18, Fe-N/CS-0.26. Where N/CS means iron nitrate nonahydrate is added, and the number of Fe-N/CS ends (0.07, 0.13, 0.18 and 0.26) means the iron content in the catalyst sample (the element content detected by XPS listed in Table 1.

2.3 Physical characteristics

The morphological feature image of the catalyst was characterized by scanning electron microscope (SEM, JEOL2100F, Japan). X-ray diffraction (XRD) (APLX-DUO, Bruker, German) and X-ray photoelectron spectroscopy (XPS) (AXIS UltraDLD) were investigated the surface structure and element composition and content of the sample. The formation of iron and carbon in the catalysts were carried out by the Raman spectra on the Thermo Fisher H31XYZE-US equipment with a laser source of 532 nm. The nitrogen adsorption and desorption isotherms of the sample were performed on ASAP-2460 (Micromeritics Instrument Corp), the specific surface area of the catalyst sample was calculated by the Brenau-Emmett-Teller (BET) method and pore size distribution was determined by Barrett-Joyner-Halenda (BJH) model.

2.4 Electrochemical characterization

The electrochemical performances of the prepared catalysts were conducted through Autolab PGSTAT302 (Metrohm) electrochemical workstation with glassy carbon (GC) electrode as the working electrode, Ag/AgCl (3.0 M KCl) as the reference electrode, and platinum wire as the counter electrode. The prepared sample by 1.0 mg was ultrasonically dispersed in a solution composed of 10.0 uL Nafion

solution as a binder and 200.0 uL water-alcohol mixed solution (the volume ratio of deionized water to ethanol is 4:1) for ultrasonic dispersion for 30 minutes to prepare catalyst ink. Then, 4 mL of catalyst ink was pipetted onto the working electrode to dry.

Cyclic Voltammetry (CV) and Linear Sweep Voltammetry (LSV) were measured in 0.1 M KOH aqueous solution, where the LSV speed range was 400 to 2000 rpm, and the scan rate was 10 mV s^{-1}. The chronoamperometry and methanol tolerance (3 M CH_3OH) experiments were carried out at a potential of 0.35 V and a rotation speed of 1600 rpm.

The electron transfer number (n) was obtained by the Koutecky-Levich (K-L) equation:

$$1/J=1/J_{Lim}+1/J_{Kin}=1/(B\omega^{1/2})+1/J_{Kin} \quad (1)$$

$$J_{Kin}=nFkC_{O2} \quad (2)$$

$$B = 0.2nFC_{O2}(D_{O2})^{2/3}\nu^{-1/6}J_{kin} = nFkC_{O2} \quad (3)$$

In the above formula, where J is the measured current density, J_{Lim} and J_{Kin} are the limiting current densities and kinetic, respectively. n is the electron transfer number, F is the Faraday constant (96,485 C mol^{-1}), C_{O2} is the bulk concentration of O_2 (1.2×10^{-6} mol cm^{-3}), D_{O2} is the diffusion coefficient of O_2 in electrolytes (1.9×10^{-5} cm^2 s^{-1}), ν is the kinematic viscosity of the electrolyte (0.01 cm^2 s^{-1}) and k is the electron-transfer rate constant. When the unit of speed is rpm, the coefficient is 0.2.

3. RESULTS AND DISCUSSION

As illustrated in Figure 1, the fiber membrane comprising carbon spheres that were codoped with different iron contents were prepared by the electrostatic spinning method. After the fiber membrane was heated and annealed, the template was removed. Then, after washing and drying, the Fe-N codoped carbon spheres (Fe-N/CS) catalysts that co-doped with different iron contents were obtained.

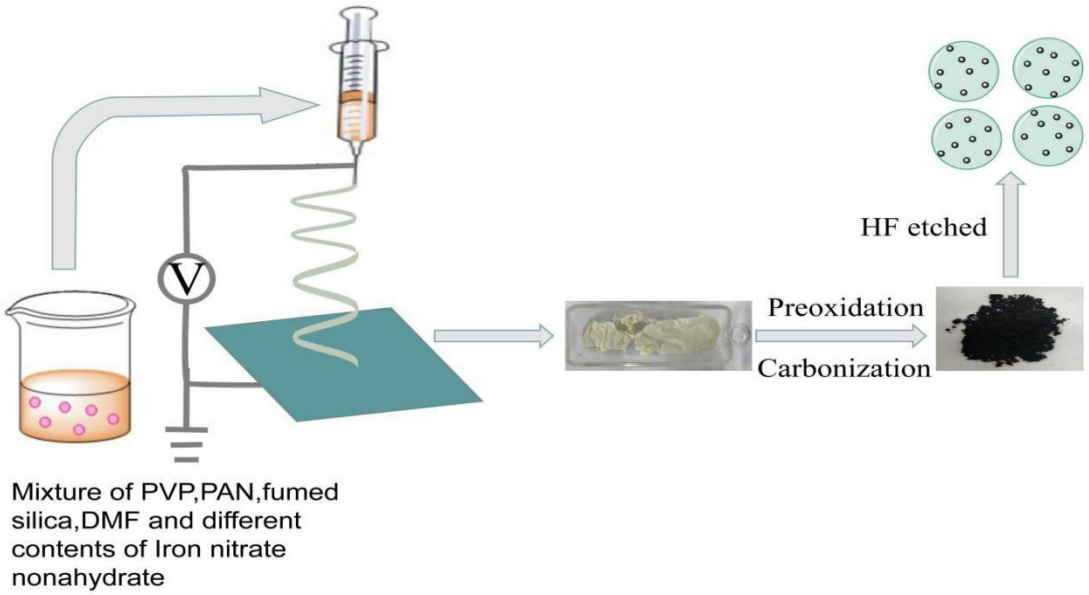

Figure 1. Schematic representation of preparation catalysts.

The morphology of the catalysts was studied. As shown in Figure 2, N/CS (Figure 2a), Fe-N/CS-0.07 (Figure 2b), Fe-N/CS-0.13 (Figure 2c), Fe-N/CS-0.18 (Figure 2d) and Fe-N/CS -0.26 (Figure 2e) all had spherical structures, but with an increase in the iron content, the morphology of the carbon spheres became slightly damaged. Their spherical shape was relatively dispersed, and their diameters were two to nine microns. To an extent, an increase in iron content led to a damaged morphology of the catalyst and even affected its performance.

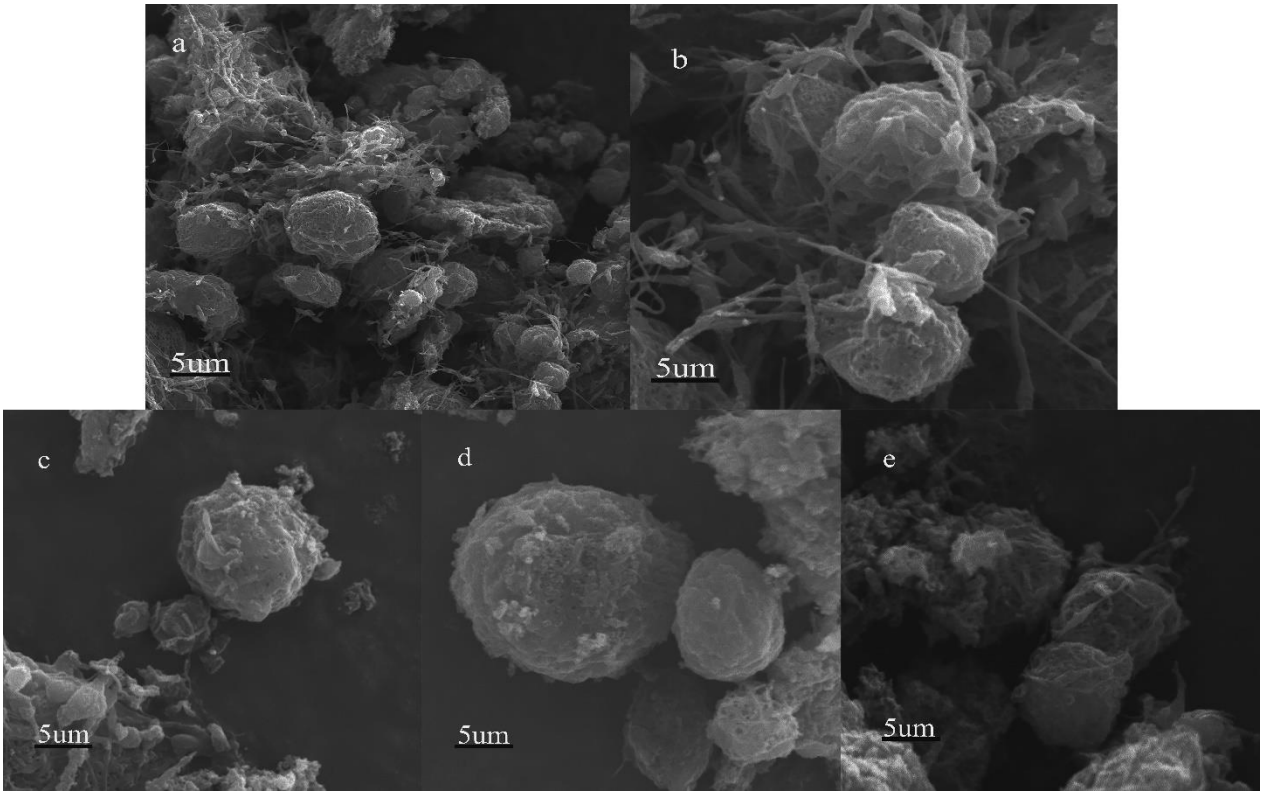

Figure 2. SEM images of (a)N/CS, (b) Fe-N/CS-0.07, (c) Fe-N/CS-0.13, (d) Fe-N/CS-0.18 and (e) Fe-N/CS -0.26.

As shown in Figure 3, the specific surface area and pore size distribution of the catalyst were obtained by performing cryogenic nitrogen adsorption-desorption and pore size distribution tests. The typical type IV curve demonstrates the mesoporous structure of the prepared catalysts. The specific surface areas of the catalyst samples were 286 m^2g^{-1} for N/CS, 222 m^2g^{-1} for Fe-N/CS-0.07, 212 m^2g^{-1} for Fe-N/CS-0.13, 163 m^2g^{-1} for Fe-N/CS-0.18, and 157 m^2g^{-1} for Fe-N/CS -0.26. With the iron content increased, the specific surface area of the catalyst gradually decreased, which was generally consistent with the SEM characterization trends. The iron doping in the catalyst damaged the morphology, and the damage to a certain extent directly affected the activity of the catalyst for oxygen reduction. This problem may have been caused by excessive metal particles blocking the pore channels in the catalyst sample or by metal chelates or their fragments bonding to the carrier surface[33]. Furthermore, the pore size distribution in Figure 3b that all the Fe-N/C maintained pore size distribution that was similar to the

nitrogen-doped carbon spheres.

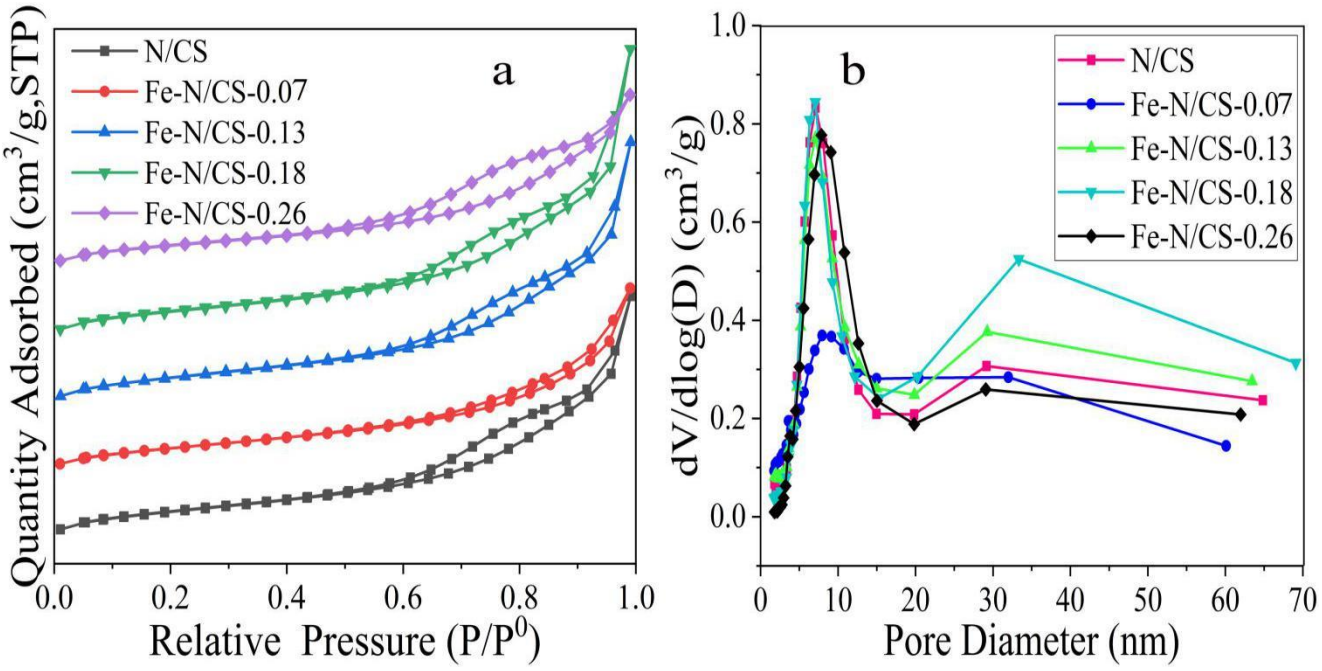

Figure 3. Nitrogen adsorption-desorption isotherm(a) and (b)pore size distribution of N/CS, Fe-N/CS-0.07, Fe-N/CS-0.13, Fe-N/CS-0.18 and Fe-N/CS -0.26.

XPS was utilized to measured the content and the types of iron and nitrogen in the different catalysts. As shown in Figure 4, Figure 5, Figure 6 and Table 1, the C 1s, O 1s, N 1s and Fe 2p signals appeared in the full XPS spectrum of the samples, indicating that iron and nitrogen were successfully doped into the catalyst. Simultaneously, to further explore the active sites of the catalyst samples, the peak orbitals of the N 1s and Fe 2p hybrid orbitals were fitted. The deconvoluted spectrum of N 1 in Figure 4, which was in conformity with the pyridine nitrogen (398.4 ± 0.2 eV), pyrrole nitrogen (399.9 ± 0.2 eV), graphite nitrogen (401.3 ± 0.2 eV) and nitrogen oxide (403.8 ± 0.2 eV). The relative content of pyridine nitrogen and graphite nitrogen in the sample was relatively high, and the presence of pyridine N and graphite N improve the ORR oxygen reduction activity of the catalyst[34-36]. As shown in Figure 6, the peaks at 712 eV and 725 eV were attributed to $2p_{3/2}$ of Fe^{2+} and $2p_{1/2}$ of Fe^{3+}, respectively, and the presence of Fe^{2+} and Fe^{3+} indicates that the iron was most likely in the form of Fe_3O_4 in the catalyst[37].

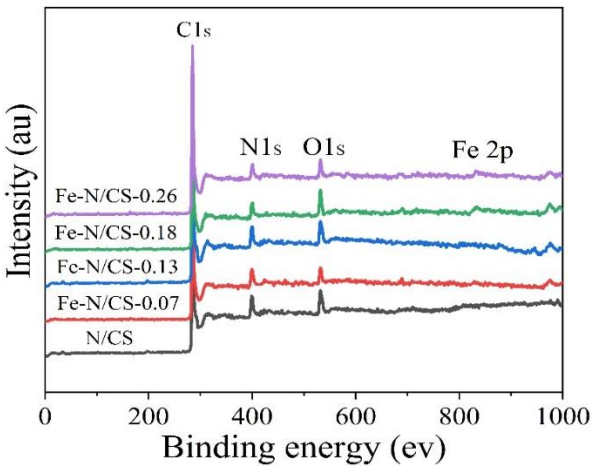

Figure 4. XPS spectra of N/CS, Fe-N/CS-0.07, Fe-N/CS-0.13, Fe-N/CS-0.18 and Fe-N/CS-0.26.

Table 1. Elemental content of five samples.

Samples	C (wt. %)	O (wt. %)	N (wt. %)	Fe (wt. %)
N/CS	86.07	5.6	8.33	0
Fe-N/CS-0.07	86.79	4.7	8.45	0.07
Fe-N/CS-0.13	83.62	7.66	8.59	0.13
Fe-N/CS-0.18	83.49	7.39	8.93	0.18
Fe-N/CS-0.26	84.9	6.31	8.54	0.26

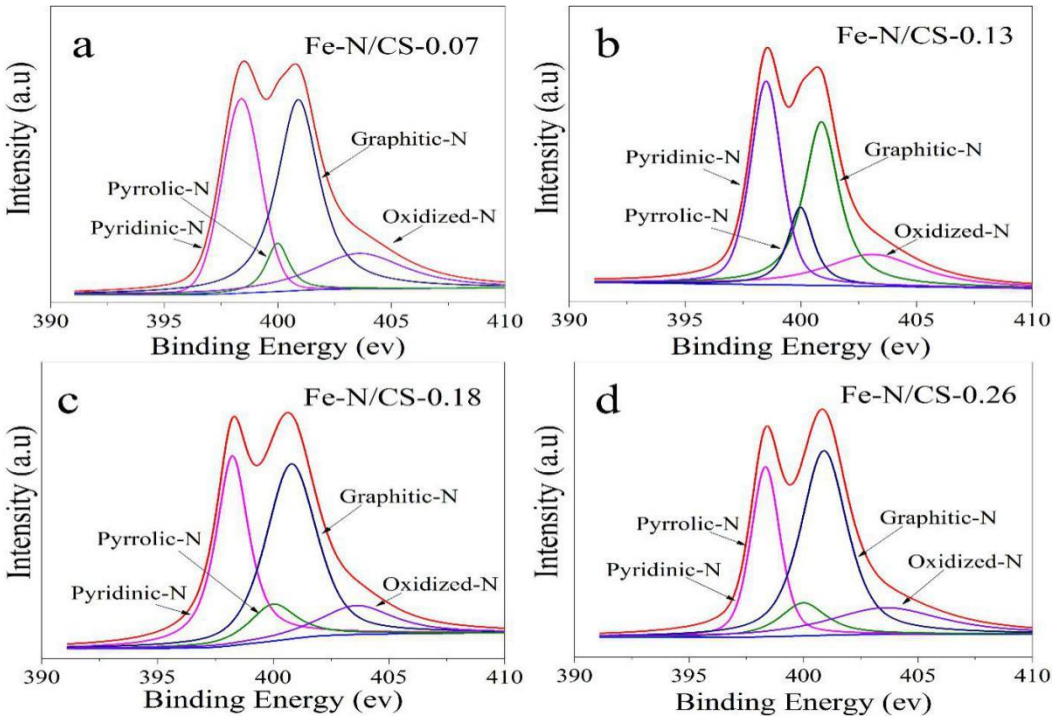

Figure 5. XPS results of N 1s Fe-N/CS-0.07(a), Fe-N/CS-0.13(b), Fe-N/CS-0.18(c) and Fe-N/CS-0.26(d).

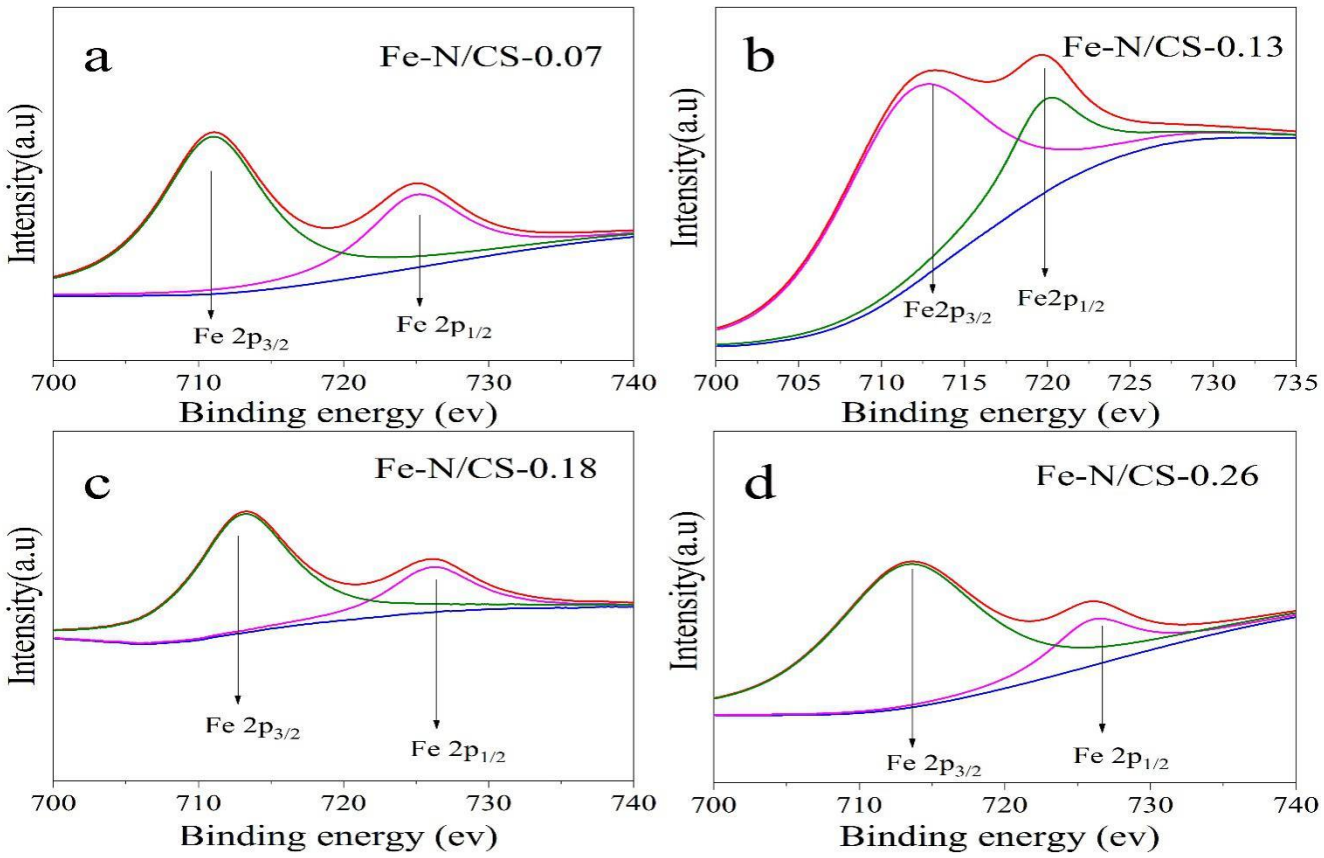

Figure 6. XPS results of Fe2p of Fe-N/CS-0.07(a), Fe-N/CS-0.13(b), Fe-N/CS-0.18(c), Fe-N/CS-0.26(d).

Figure 7a showed the XRD characterization results of five samples. Except for the amorphous peak of carbon, none of the five catalyst samples showed obvious iron characteristic peaks, which may indicate that the iron content is relatively low and uniformly dispersed in the catalyst sample[38, 39].

The Raman spectrum could be characterized by the degree of graphitization and defect structure of carbon. As shown in Figure 7b, the samples have two intense peaks at approximately 1350 cm^{-1} and 1580 cm^{-1}. The peak at 1580 cm^{-1} corresponded to the characteristic vibration peak in the sp2 bonded carbon plane, which reflected the graphitized structure of the carbon material, represented by G band. The ratio of the D band to the G band (ID/IG) indicated the defect degree of carbon material[40]. The results showed that the (I_D/I_G) ratios of the five catalysts were very high and had values of 2.98, 3.13, 3.09, 3.16, and 3.22. A higher ID/IG value indicated that the structure of the catalyst was disordered and accompanied by a plentiful defects, which corresponded to the XRD results of amorphous carbon. This large number of disordered sites may have provided additional catalytically active sites that were conducive to oxygen reduction.

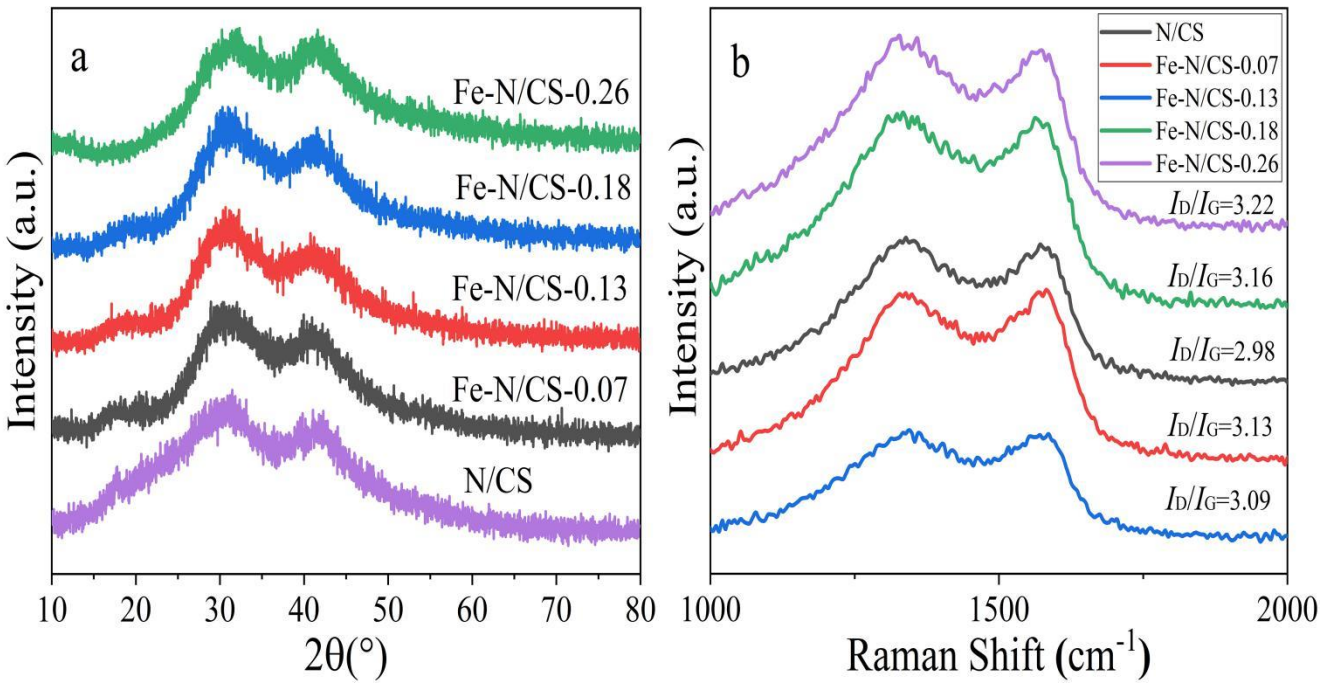

Figure 7. (a)XRD patterns and (b) Raman spectra of N/CS, Fe-N/CS-0.07, Fe-N/CS-0.13, Fe-N/CS-0.18 and Fe-N/CS -0.26.

To further investigate the influence of different iron contents on the oxygen reduction performance of the catalyst, the cyclic voltammetry curves (CV) of the catalysts were carried out in 0.1 M KOH solution saturated with O_2. Nernst equation was used to convert the Ag/AgCl potential into RHE, E (vs. RHE) = $E_{Ag/AgCl}$ + pH × 0.059 + 0.210[41,42].

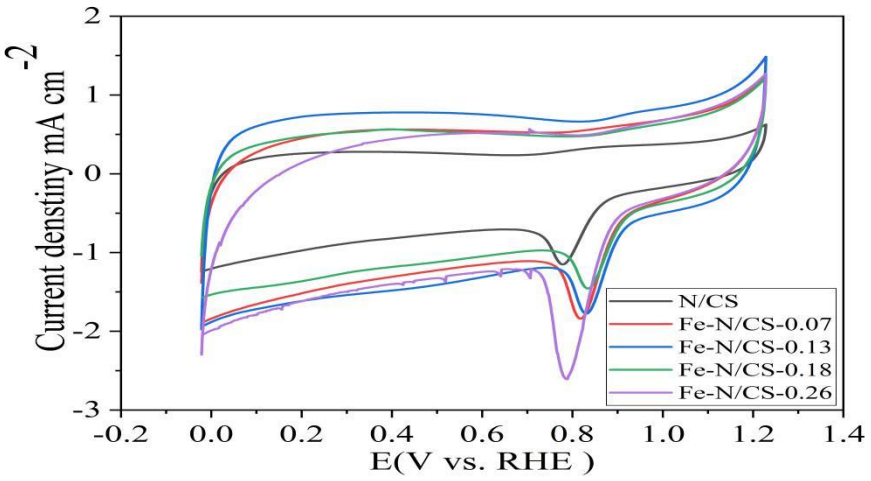

Figure 8. CV curves of N/CS, Fe-N/CS-0.07, Fe-N/CS-0.13, Fe-N/CS-0.18 and Fe-N/CS -0.26 in O_2-saturated 0.1 M KOH electrolyte.

Figure 8 indicated that all the catalysts had significant oxygen reduction activity. Compared with the peaks from N/CS (0.779 V) Fe-N/CS-0.07 (0.825 V), Fe-N/CS-0.13 (0.829 V) and Fe-N/CS -0.26(0.787 V) of the other four catalysts, Fe-N/CS-0.18 showed the most positive oxygen reduction peak

position, with a value of 0.837 V. This indicates that Fe-N/CS-0.18 has the best ORR performance herein. From the analysis of the electrochemical properties, when the content of iron was low, the activity of the catalyst increased with an increase in the iron content, and when the content of iron reached a certain value, the activity decreased. It may be that too much metal formed metal clusters, which were not conducive to oxygen reduction[43-45].

To further explore the oxygen reduction performance and kinetics of the iron-nitrogen codoped spherical carbon catalyst, a linear cyclic voltammetry (LSV) test was performed on the sample, and a K-L curve was calculated. The results are shown in Figure 9, Figure 10 and Table 2. The initial potential, half-wave potential, limiting current density and electron transfer number of the catalyst prepared in this experiment can be obtained from Table 2. As shown in Table 2, when the content of iron was less than 0.18%, the oxygen reduction performance increased as the iron content increased, but when the content of iron exceeded 0.18% and reached 0.26%, the performance of the catalyst began to decline. Among them, Fe-N/CS-0.18 had the most positive initial potential, half-wave potential and maximum limiting current density, which declared that when the content of iron was 0.18%, the performance of the catalyst was the best herein. For comparison, commercial Pt/C was tested under the same conditions and Figure 10 and Table 2 indicated that Fe-N/CS-0.18 possessed a better catalytic activity.

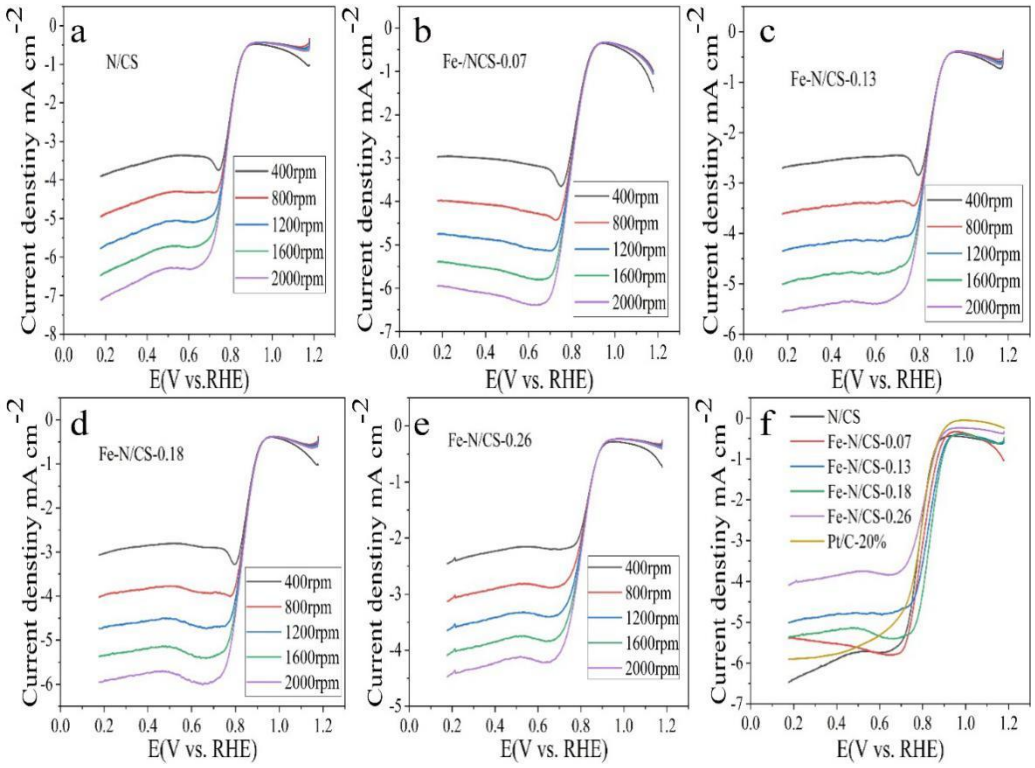

Figure 9. LSV curves of the five samples in O_2 saturated 0.1 M KOH with a scan rate of 10 mV s^{-1}; (f)Five samples and Pt/C in O_2 saturated 0.1 M KOH at 1600 rpm.

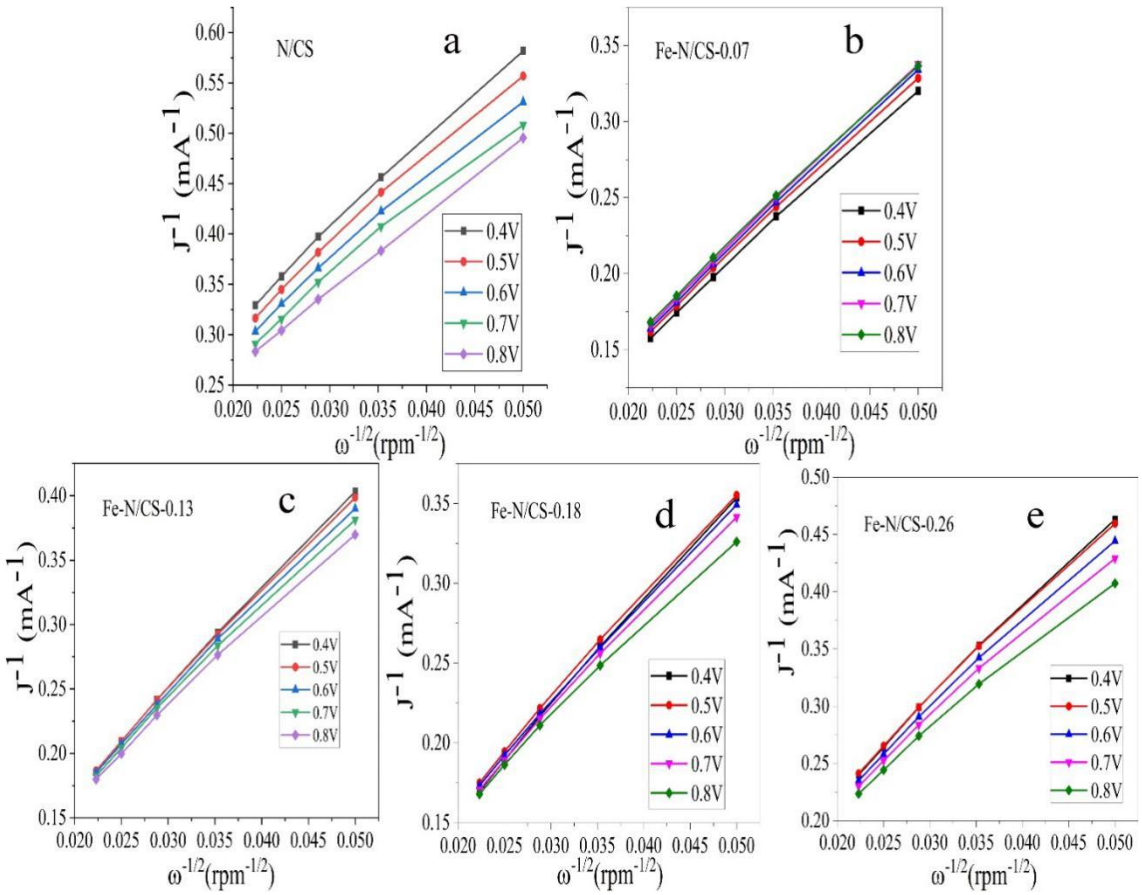

Figure 10. K-L plots of N/CS(a), Fe-N/CS-0.07(b), Fe-N/CS-0.13(c) and Fe-N/CS-0.18(d), Fe-N/CS-0.26(e).

Table 2. Electrocatalytic performance comparison of five samples and commercial Pt/C 20% catalyst.

Samples	Initial potential (V vs. RHE)	Half-wave potential (V vs. RHE)	Limiting current density (mA/cm^2)	Electron transfer number (n)
N/CS	0.935	0.779	6.4	4
Fe-N/CS-0.07	0.931	0.808	5.4	4
Fe-N/CS-0.13	0.960	0.833	5	4
Fe-N/CS-0.18	0.970	0.842	5.5	4
Fe-N/CS-0.26	0.937	0.814	4	3.8
Pt/C -20%	0.968	0.800	6	4

The initial potential and half-wave potential of Fe-N/CS-0.18 were 0.970 V and 0.842 V, respectively, which are better than those for commercial Pt/C (0.970 V and 0.798 V, respectively), indicating its excellent oxygen reduction performance. In order to compare the ORR activity of this study with other similar non-noble metal electrocatalysts, some literature [32, 46-50] were investigated and

the results are listed in Table 3. Although the onset potential of Fe-N/C-0.18 is slightly lower than that reported in some literature, the half-wave potential is more positive than those reported. Summarily, the iron-nitrogen co-doped carbon electrocatalyst prepared in this study performed better Oxygen activity and considerable prospects.

Table 3. Comparison of ORR activity of Fe-N/MC-0.18 and other Fe-based electrocatalysts.(With Ag/AgCl as the reference electrode, the electrocatalyst was tested in 0.1 M KOH at 1600 rpm).

Samples	Initial potential (V vs. RHE)	Half-wave potential (V vs. RHE)	References
Fe-N/MCS-181	0.959	0.832	[32]
Fe/Fe_2O_3 @Fe-N-C-1000	0.947	0.817	[46]
Fe@EY-NH3	0.90	0.81	[47]
Fe@FeNx	0.85	0.75	[48]
Fe-Co-N-C	0.90	0.76	[49]
FeNC/MXene	1.00	0.81	[50]
Fe-N/CS-0.18	0.970	0.842	This work

The durability and methanol tolerance of the catalysts were tested (Figure 11), and it was found that after 10000 s, the Fe-N/CS-007, Fe-N/CS-0.13, Fe-N/CS-0.18, and Fe-N/CS-0.26 samples maintained 91.2%, 86.4%, 90.6%, and 85.2% of the current, which was better than commercial Pt/C (84.2%) in Figure 11(a). Moreover, after adding methanol catalyst as shown in Figure 11(b-f), the stability of N/CS and Fe-N/CS catalysts decreased slightly, while the commercial Pt/C dropped sharply. In particular, the Fe-N/CS-0.18 sample had more stable electrochemical properties than the commercial Pt/C in Figure 11(e).

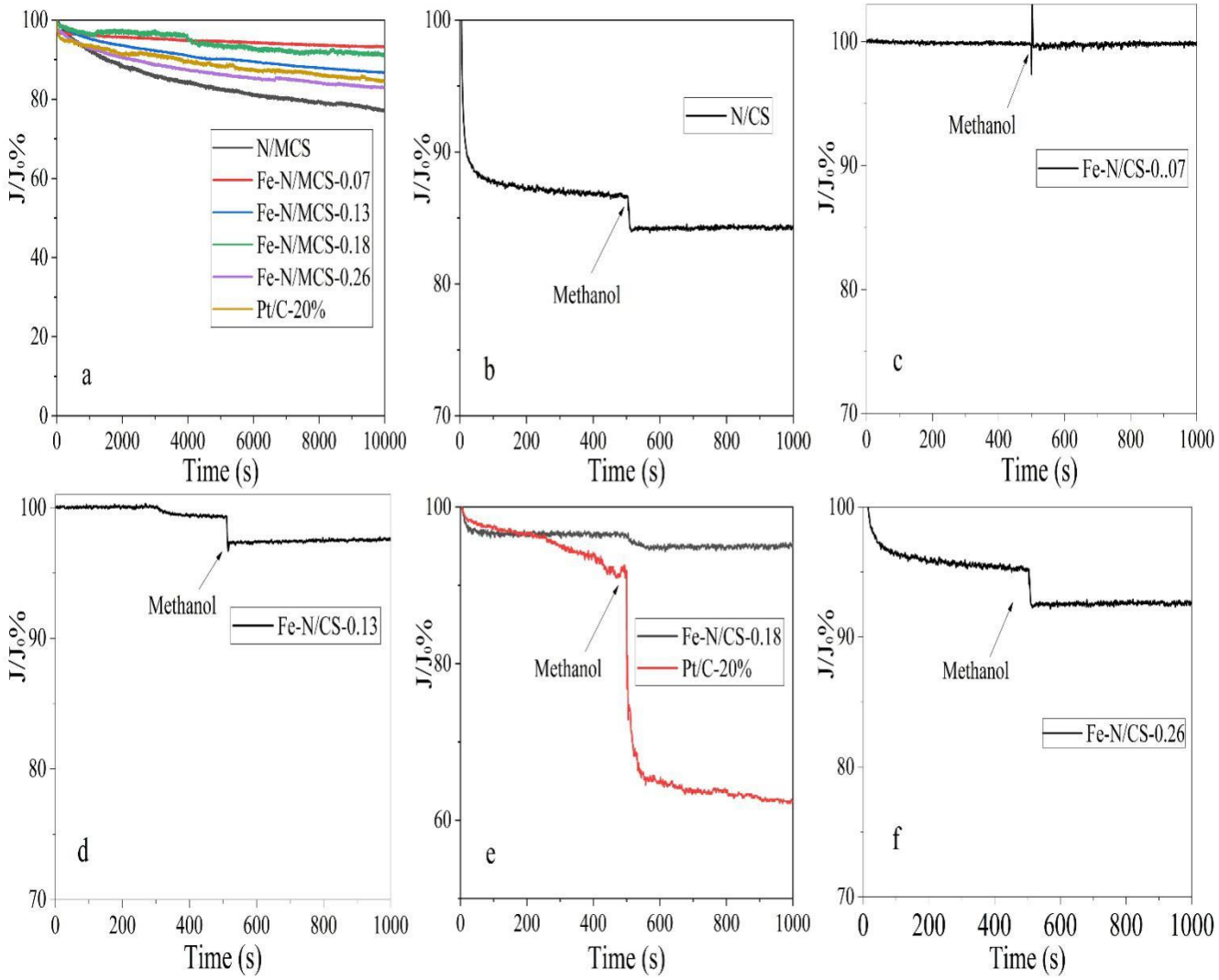

Figure 11. The chronoamperometric responses of N/CS, Fe-N/CS-0.07, Fe-N/CS-0.13, Fe-N/CS-0.18, Fe-N/CS-0.26 and commercial 20%-Pt/C at -0.35 V in the O_2-saturated 0.1 M KOH(a). Chronoamperometric responses of the N/CS(b), Fe-N/CS-0.07(c), Fe-N/CS-0.13(d), Fe-N/CS-0.26(f), Fe-N/CS-0.18 and Pt/C-20%(e) with 3 M methanol added at 500 s.

4. CONCLUSION

In summary, by changing the content of the added iron precursor, the amount of iron doped in the iron-nitrogen spherical carbon catalyst has been changed. Among the prepared iron and nitrogen co-doped catalysts, the Fe-N/CS-0.18 sample (iron content 0.18%) had the best oxygen reduction performance. The Fe-N/CS-0.18 had a starting potential of 0.970 V and a half-wave potential of 0.842 V, which is even better than that for a commercial Pt/C (0.970 V and 0.798 V, respectively). In addition, its limiting current density of 5.5 mA/cm^2 is slightly lower than the 6 mA/cm^2 value for a commercial Pt/C. However, its stability and methanol tolerance are better than those of commercial Pt/C. Therefore, the prepared Fe-N/CS-0.18 catalyst has a considerable application prospect.

ACKNOWLEDGEMENTS
This project was financially supported by the National Key R&D Program of China (2020YFB1505500 and 2020YFB1505503) and Shanghai Science and Technology Commission science and technology innovation action plan (20511103800 and 20511103803). Meanwhile, this work was also got help from the State Key Laboratory of Fluorinated Functional Membrane Materials.

References

1. G.A. Giffin, G.M. Haugen, S.J. Hamrock, V. Di Noto, *J. Am. Chem. Soc.,* 135 (2013) 822.
2. O.T. Holton, J.W. Stevenson, *Platin Met Rev*, 57 (2013) 259.
3. M. Lopez-Haro, L. Guetaz, T. Printemps, A. Morin, S. Escribano, P.H. Jouneau, P. Bayle-Guillemaud, F. Chandezon, G. Gebel, *Nat. Commun.,* 5 (2014)5229.
4. Y. Wang, K.S. Chen, J. Mishler, S.C. Cho, X.C. Adroher, *Appl. Energy,* 88 (2011) 981.
5. P. Zhou, C.W. Wu, G.J. Ma, *J. Power Sources*, 163 (2007) 874.
6. Z. Huang, H.Y. Pan, W.J. Yang, H.H. Zhou, N. Gao, C.P. Fu, S.C. Li, H.X. Li, Y.F. Kuang, *Acs Nano*, 12 (2018) 208.
7. M. Prasanna, H.Y. Ha, E.A. Cho, S.A. Hong, I.H. Oh, *J. Power Sources*, 131 (2004) 147.
8. D.J. Seo, W.L. Yoon, Y.G. Yoon, S.H. Park, G.G. Park, C.S. Kim, *Electrochim. Acta,* 50 (2004) 719.
9. M.X. Song, Y.H. Song, W.B. Sha, B.S. Xu, J.J. Guo, Y.C. Wu, *Catalysts,* 10 (2020) 23.
10. X. Zhou, J. Qiao, L. Yang, J. Zhang, *Adv. Energy Mater.,* 4 (2014) 1301523.
11. X. Han, F. Cheng, T. Zhang, J. Yang, Y. Hu, J. Chen, *Adv. Mater.,* 26 (2014) 2047.
12. L.C. Mao, K. Fu, J.H. Jin, S.L. Yang, G. Li, *Int. J. Hydrog. Energy*, 44 (2019) 18083.
13. J. Zhang, K. Sasaki, E. Sutter, R.R. Adzic, *Science*, 315 (2007) 220.
14. C.K. Acharya, D.I. Sullivan, C.H. Turner, *J. Phys. Chem. C*, 112 (2008) 13607.
15. X.L. Zhao, X.X. Yang, M.Y. Wang, S. Hwang, S. Karakalos, M.J. Chen, Z. Qiao, L. Wang, B. Liu, Q. Ma, D.A. Cullen, D. Su, H.P. Yang, H.Y. Zang, Z.X. Feng, G. Wu, *Appl. Catal. B-Environ.,* 279 (2020) 11.
16. G.J.K. Acres, J.C. Frost, G.A. Hards, R.J. Potter, T.R. Ralph, D. Thompsett, G.T. Burstein, G.J. Hutchings, *Catal. Today,* 38 (1997) 393.
17. D.S. Su, G.Q. Sun, *Angew. Chem.-Int. Edit.,* 50 (2011) 11570.
18. Z. Chen, D. Higgins, A. Yu, L. Zhang, J. Zhang, *Energy Environ. Sci.,* 4 (2011) 3167.
19. D. Banham, S. Ye, K. Pei, J. Ozaki, T. Kishimoto, Y. Imashiro, *J. Power Sources*, 285 (2015) 334.
20. C. Dominguez, F.J. Perez-Alonso, M.A. Salam, J.L.G. de la Fuente, S.A. Al-Thabaiti, S.N. Basahel, M.A. Pena, J.L.G. Fierro, S. Rojas, *Int. J. Hydrog. Energy*, 39 (2014) 5309.
21. H. Tian, C. Zhang, P.P. Su, Z.F. Shen, H. Liu, G.X. Wang, S.M. Liu, J. Liu, *J. Energy Chem.*, 40 (2020) 137.
22. W.Y. Noh, J.H. Lee, J.S. Lee, *Appl. Catal. B-Environ.,* 268 (2020) 8.
23. H.Z. Zou, Z.Y. Chen, X. Xiong, Y.Y. Sun, S.P. Pei, Y.M. Zhang, *Int. J. Electrochem. Sci.,* 15 (2020) 2039.
24. J. Zhang, X.M. Song, P. Li, S. Wang, Z.X. Wu, X.E. Liu, *Catalysts*, 8 (2018) 13.
25. X.L. Yan, Y.C. Yao, Y. Chen, *Nanoscale Res. Lett.,* 13 (2018) 7.
26. Z.Y. Wu, X.X. Xu, B.C. Hu, H.W. Liang, Y. Lin, L.F. Chen, S.H. Yu, *Angew. Chem.-Int. Edit.,* 54 (2015) 8179.
27. A. Li, S.A. Nicolae, M. Qiao, K. Preuss, P.A. Szilágyi, A. Moores, M.M. Titirici, *ChemCatChem*, 11 (2019) 3600.
28. A. Zitolo, V. Goellner, V. Armel, M.T. Sougrati, T. Mineva, L. Stievano, E. Fonda, F. Jaouen, *Nat. Mater.,* 14 (2015) 937.
29. L. Shang, H.J. Yu, X. Huang, T. Bian, R. Shi, Y.F. Zhao, G.I.N. Waterhouse, L.Z. Wu, C.H. Tung,

T.R. Zhang, *Adv. Mater.*, 28 (2016) 1668.
30. A. P. Kishan and E. M. Cosgriff-Hernandez, J. Biomed. *Mater. Res., Part A,* 105(2017) 2892.
31. X. Lu, C. Wang, F. Favier, N. Pinna, *Adv. Energy Mater.*, 7 (2017)1601301.
32. H.Z. Zou, S.P. Pei, Z.S. Zhou, Z.Y. Chen, X. Xiong, Y.Y. Sun, Y.M. Zhang, *Rsc Advances*, 10 (2020) 779.
33. G.Q. Sun, J.T. Wang, S. Gupta, R. Savinell, *J Appl Electrochem*, 31 (2001) 1025.
34. Z. Chen, A.P. Yu, R. Ahmed, H.J. Wang, H. Li, Z.W. Chen, *Electrochim. Acta*, 69 (2012) 295.
35. E.J. Biddinger, U.S. Ozkan, *J. Phys. Chem. C*, 114 (2010) 15306.
36. Z.Q. Luo, S.H. Lim, Z.Q. Tian, J.Z. Shang, L.F. Lai, B. MacDonald, C. Fu, Z.X. Shen, T. Yu, J.Y. Lin, *J. Mater. Chem.*, 21 (2011) 8038.
37. D. Zhou, L.P. Yang, L.H. Yu, J.H. Kong, X.Y. Yao, W.S. Liu, Z.C. Xu, X.H. Lu, *Nanoscale*, 7 (2015) 1501.
38. S.F. Fu, C.Z. Zhu, J.H. Song, M.H. Engelhard, B.W. Xiao, D. Du, Y.H. Lin, *Chem-Eur. J.*, 23 (2017) 10460.
39. K. Kakaei, A. Balavandi, *J. Colloid Interface Sci*., 490 (2017) 819.
40. Y.Y. Gao, L. Wang, G.Z. Li, Z.R. Xiao, Q.F. Wang, X.W. Zhang, *Int. J. Hydrog. Energy*, 43 (2018) 7893.
41. B.B. Blizanac, P.N. Ross, N.M. Markovic, *J. Phys. Chem. B*, 110 (2006) 4735.
42. H. Park, S. Oh, S. Lee, S. Choi, M. Oh, *Appl. Catal. B Environ.*, 246 (2019) 322.
43. M. Lefèvre, J.P. Dodelet, P. Bertrand, *J. Phys. Chem. B*, 104 (2000) 11238.
44. M. Bron, S. Fiechter, M. Hilgendorff, P. Bogdanoff, *J. Appl. Electrochem*., 32 (2002) 211.
45. H. Wang, R. Cote, G. Faubert, D. Guay, J.P. Dodelet, *J. Phys. Chem. B*, 103 (1999) 2042.
46. Y. Zang, H. Zhang, X. Zhang, R. Liu, S. Liu, G. Wang, Y. Zhang, H. Zhao, *Nano Res*., 9 (2016) 2123.
47. L. Qin, X.C. Yu, J. Li, S.Y. Li, Y.Y. Liu, P.C. Qian, J.C. Wang, S. Wang, H.L. Jin, *Int. J. Electrochem. Sci.*, 15 (2020) 9168.
48. Y. Chen, Z. Shi, Z. Wang, C. Wang, J. Feng, B. Pang, Q. Sun, L. Yu, L. Dong, *J. Alloys Comp.*, 829 (2020) 154558.
49. L. Osmieri, C. Zafferoni, L. Wang, A.H.A. Monteverde Videla, A. Lavacchi, S. Specchia, *ChemElectroChem*, 5 (2018) 1954.
50. Y.Y. Wen, C. Ma, Z.T. Wei, X.X. Zhu, Z.X. Li, *Rsc Advances*, 9 (2019) 13424.